

End-to-end Analysis and Design of a Drone Flight Controller

Zhuoqun Cheng, Richard West, *Senior Member, IEEE*, and Craig Einstein

Abstract—Timing guarantees are crucial to embedded and cyber-physical applications that must bound the end-to-end delay between sensing, processing and actuation. For example, in a flight controller for a multirotor drone, the data from a gyro or inertial sensor must be gathered and processed to determine the attitude of the aircraft. Sensor data fusion is followed by control outputs that alter rotor speeds to adjust the drone's flight. If the processing pipeline between sensor input and actuation is not bounded, the drone will lose control and possibly fail to maintain flight.

This paper describes a composable pipe model for sensor data processing and actuation tasks. The pipe model is used to analyze two end-to-end semantics: freshness and reaction time. We provide a mathematical framework to derive feasible task periods and budgets that satisfy both schedulability and end-to-end timing requirements. We demonstrate the applicability of our design approach by using it to port the Cleanflight flight controller firmware to our in-house real-time operating system (RTOS) called Quest. Experiments show that Cleanflight ported to Quest is able to achieve end-to-end latencies within the predicted time bounds derived by analysis.

Index Terms—real-time systems, end-to-end timing analysis, flight controller

I. INTRODUCTION

Common to many embedded and cyber-physical applications is a communicating task *pipeline*, to acquire and process sensor data and produce outputs that control actuators. For example, a multirotor unmanned aerial vehicle (a.k.a. UAV or drone) typically processes inertial sensors to estimate its current attitude¹, and then uses a control function to adjust rotor speeds, which adapt the flight path.

The objective of our work is to develop a system that supports real-time task pipelines with end-to-end timing guarantees. As a case study, we focus on the implementation of a real-time flight controller that is the basis for an autonomous drone. Our first step is to refactor a popular flight control firmware, called Cleanflight [1] for use with our in-house real-time operating system (RTOS) called Quest [2]. Cleanflight [1] is used on racing drones that are operated by humans via radio-control. By porting Cleanflight to run as a real-time application on Quest, we have the opportunity to integrate it with additional functionality necessary for a fully autonomous flight management system. The aim is to replace radio-control with on-board tasks that perform configurable flight missions,

such as aerial photography, package delivery, and search and rescue.

Using a multirotor drone flight controller as an example, the challenge is to determine the required task timing constraints necessary for end-to-end latency guarantees. Sensor data must be sampled and processed at a minimum rate to ensure the drone is operating according to the most recent estimates of its attitude, direction, altitude, and speed. Similarly, the rotor speeds must be updated within certain time bounds to be relevant to the current sensor readings. For this reason, we define two end-to-end timing constraints, in terms of sensor data *freshness* and actuator *reaction* time that constrain the problem of composing a feasible task pipeline.

In Quest, each pipelined task is a separate thread of control, mapped to a virtual CPU (VCPU). A VCPU is guaranteed C time units of service every period, T , when its corresponding thread is runnable. This is achieved by treating every VCPU as a bandwidth-preserving server [3]. Thus, for a set of tasks in a pipeline, each mapped to a separate VCPU, the problem is to determine a valid set of budgets and periods that ensure end-to-end freshness and reaction times, while satisfying the schedulability of all VCPUs.

The contributions of this paper are: 1) a composable pipe model that guarantees bounded end-to-end processing and communication delay amongst a set of independently activated tasks assigned to bandwidth-preserving servers; 2) a method to derive task periods and budgets from given end-to-end timing constraints in the application design stage; 3) the re-implementation and evaluation of the Cleanflight flight controller on the Quest real-time operating system.

The following section provides background to the execution model used in this paper. Section III describes the end-to-end timing analysis of our proposed composable pipe model. Section IV shows how the end-to-end time is leveraged in the application design stage, while Section V details the re-implementation and evaluation of Cleanflight on the Aero board. Related work is discussed in Section VI, followed by conclusions and future work in Section VII.

II. EXECUTION MODEL

This paper is motivated by our objective to implement an autonomous flight management system for multirotor drones. An autonomous drone is one that is able to reason about and adapt to changes in its surroundings, while accomplishing mission objectives without remote assistance from a human being. As part of this effort, we have undertaken a port of the Cleanflight firmware to the Quest real-time operating

Z. Cheng, R. West and C. Einstein are in the Computer Science Department, Boston University, Boston, MA 02215.

This article was presented in the International Conference on Embedded Software 2018 and appears as part of the ESWEK-TCAD special issue.

¹The attitude is the orientation of the drone relative to a reference frame such as earth.

system. The core software components of Cleanflight consist of sensor and actuator drivers, a PID controller, the Mahony Attitude and Heading Reference (AHRS) algorithm, various communication stacks, and a logging system.

A. Task Model

We model the flight controller program as a set of real-time periodic tasks $\{\tau^1, \tau^2, \dots, \tau^n\}$, whose initial release times are arbitrary. Each task τ^j is characterized by its worst-case execution time e^j , period T^j , and a deadline that is equal to period. Additionally, each task communicates with zero or more successors and predecessors, to exchange and process data.

e^j and T^j are determined during the design stage and are fixed at runtime. e^j is usually profiled off-line under the worst-case execution condition. Deciding the value of T^j is a challenging process, which is the major topic of this paper. It mainly depends on the end-to-end latency constraints and the schedulability test. All the periodic tasks are implemented using user-level threads.

Apart from user-level threads, there are kernel threads dedicated to I/O interrupts, which originate primarily from the SPI and I2C bus in Cleanflight. Quest executes interrupts in a deferrable thread context, having a corresponding time budget. This way, the handling of an interrupt does not steal CPU cycles from a currently running, potentially time-critical task.

B. Scheduling Model

Threads in Quest are scheduled by a two-level scheduling hierarchy, with threads mapped to virtual CPUs (VCPUs) that are mapped to physical CPUs. Each VCPU is specified a processor capacity reserve [4] consisting of a budget capacity, C , and period, T . The value of C and T are determined by the e and T of the task mapped to the VCPU. A VCPU is required to receive at least C units of execution time every T time units when it is runnable, as long as a schedulability test [5] is passed when creating new VCPUs. This way, Quest's scheduling subsystem guarantees temporal isolation between threads in the runtime environment.

Conventional periodic tasks are assigned to Main VCPUs, which are implemented as Sporadic Servers [3] and scheduled using Rate-Monotonic Scheduling (RMS) [6]. The VCPU with the smallest period has the highest priority. Instead of using the Sporadic Server model for both main tasks and bottom half threads, special I/O VCPUs are created for threaded interrupt handlers. Each I/O VCPU operates as a Priority Inheritance Bandwidth preserving Server (PIBS) [7]. A PIBS uses a single replenishment to avoid fragmentation of replenishment list budgets caused by short-lived interrupt service routines (ISRs). By using PIBS for interrupt threads, the scheduling overheads from context switching and timer reprogramming are reduced [8].

C. Communication Model

Control flow within the flight controller is influenced by the path of data, which originates from sensory inputs and

ends with actuation. Inputs include inertial sensors, optional cameras and GPS devices, while actuators include motors that affect rotor speeds and the attitude of the drone. Data flow involves a pipeline of communicating tasks, leading to a communication model characterized by: (1) the interarrival times of tasks in the pipeline, (2) inter-task buffering, and (3) the tasks' access pattern to communication buffers.

Periodic versus Aperiodic Tasks. Aperiodic tasks have irregular interarrival times, influenced by the arrival of data. Periodic tasks have fixed interarrival times and operate on whatever data is available at the time of their execution. A periodic task implements asynchronous communication by not blocking to await the arrival of new data.

Register-based versus FIFO-based Communication. A FIFO-based shared buffer is used in scenarios where *data history* is an important factor. However, in a flight controller, *data freshness* outweighs the preservation of the full history of all sampled data. For example, the motor commands should always be computed from the latest sensor data and any stale data should be discarded. Moreover, FIFO-based communication results in loosely synchronous communication: the producer is suspended when the FIFO buffer is full and the consumer is suspended when the buffer is empty. Register-based communication achieves fully asynchronous communication between two communicating parties using Simpson's four-slot algorithm [9].

Implicit versus Explicit Communication. Explicit communication allows access to shared data at any time point during a task's execution. This might lead to data inconsistency in the presence of task preemption. A task that reads the same shared data at the beginning and the end of its execution might see two different values, if it is preempted between the two reads by another task that changes the value of the shared data. Conversely, the implicit communication model [10] essentially follows a read-before-execute paradigm to avoid data inconsistency. It mandates a task to make a local copy of the shared data at the beginning of its execution and to work on that copy throughout its execution. Simpson's four-slot algorithm [9] ensures the *read* and *write* stages avoid data corruption without blocking.

This paper assumes a periodic task model, as this simplifies timing analysis. Applications such as Cleanflight implement periodic tasks to sample data and perform control operations. Quest also adopts register-based, implicit communication for data freshness and consistency.

III. END-TO-END TIMING ANALYSIS

In this section, we first distinguish two different timing semantics for end-to-end communication, which will be used as the basis for separate timing analyses. Secondly, we develop a composable pipe model for communication, which is derived from separate latencies that influence end-to-end delay. Lastly, we use the pipe model to derive the worst-case end-to-end communication time under various situations.

A. Semantics of End-to-end Time

To understand the meaning of end-to-end time, consider the following two constraints for a flight controller:

- Constraint 1: a *change* in motor speed must be within 2 ms of the gyro sensor reading that caused the change.
- Constraint 2: an *update* to a gyro sensor value must be within 2 ms of the corresponding update in motor speed.

The values before and after a *change* differ, whereas they may stay the same before and after an *update*. These semantics lead to two different constraints. To appreciate the difference, imagine the two cases in Table I. In Case 1, the task that reads the gyro runs every 10 ms and the one that controls the motors runs every 1 ms. Case 1 is guaranteed to meet Constraint 1 because the motor task runs more than once within 2 ms, no matter whether the gyro reading changes. However, it fails Constraint 2 as the gyro task is not likely to run even once in an interval of 2 ms. Conversely, Case 2 is guaranteed to meet Constraint 2 but fails Constraint 1 frequently.

	Gyro Period	Motor Period
Case 1	10 ms	1 ms
Case 2	1 ms	10 ms

TABLE I
EXAMPLE PERIODS

This example demonstrates the difference between the two semantics of end-to-end time, defined as follows:

- **Reaction time** is the time it takes for a sample of input data to flow through the system, and is affected by the period of each consumer in a pipeline. A reaction timing constraint bounds the time interval between a sensor input and the *first corresponding* actuator output.
- **Freshness time** is the interval within which a sampled data input has influence on the system, and is affected by the period of each producer in a pipeline. A freshness timing constraint bounds the interval between a sensor input and the *last corresponding* actuator output.

Constraint 1, above, is a constraint on reaction time, while Constraint 2 is on freshness time. We perform analysis of the two semantics of time in Section III-E2 and III-E3, respectively.

B. Latency Contributors

The end-to-end communication delay is influenced by several factors, which we will identify as part of our analysis. To begin, we first consider the end-to-end communication pipeline illustrated as a task chain in Figure 1. Task τ_1 reads input data D_{in} over channel Ch_{in} , processes it and produces data D_1 . Task τ_2 reads D_1 and produces D_2 , and τ_3 eventually writes output D_{out} to channel Ch_{out} after reading and processing D_2 .

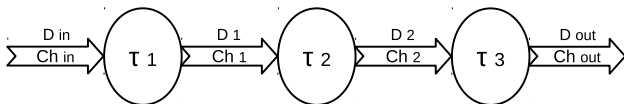


Fig. 1. Task Chain

Each task handles data in three stages, *i.e.*, read, process and write. The end-to-end time should sum the latency of each stage in the task chain. Due to the asynchrony of

communication, however, we also need to consider one less obvious latency, which is the waiting time it takes for an intermediate output to be read in as input, by the succeeding task in the chain. In summary, the latency contributors are classified as follows:

- **Processing latency** represents the time it takes for a task to translate a raw input to a processed output. The actual processing latency depends not only on the absolute processing time of a task without interruption, but also on the service constraints (*i.e.*, CPU budget and period of the VCPU) associated with the task.
- **Communication latency** represents the time to transfer data over a channel. The transfer data size, channel bandwidth, propagation delay, and communication protocol overheads all contribute to the overall latency. Since our communication model is asynchronous and register-based as described in Section II, queuing latency is not a concern of this work.
- **Scheduling latency** represents the time between the arrival of data on a channel from a sending task and when the receiving task begins reading that data. The scheduling latency depends on the order of execution of tasks in the system, and therefore has significant influence on the end-to-end communication delay.

C. The Composable Pipe Model

In Section III-B, we identified the factors that influence end-to-end communication delay. Among them, the absolute processing time and the transfer data size are determined by the nature of the task in question. To capture the rest of the timing characteristics, we develop a composable pipe model, leveraging the scheduling approach described in Section II-B. A task and pipe have a one-to-one relationship, as illustrated in Figure 2.

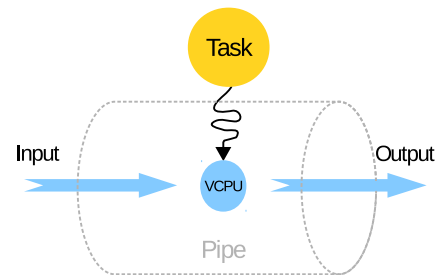


Fig. 2. Illustration of a Pipe

A pipe has one *pipe terminal* and two *pipe ends*, with one end for input and the other for output. A pipe terminal is represented by a VCPU, guaranteeing at least C units of execution time every T time units when runnable. Pipe terminals are associated with conventional tasks bound to Main VCPUs and kernel control paths (including interrupt handlers and device drivers) bound to I/O VCPUs, as described in Section II-B.

A pipe end is an interface to a communication channel, which is either an I/O bus or shared memory. The pipe end's propagation delay is assumed negligible, while the

transmission delay is modeled by the bandwidth parameter, W , of the communication channel. δ is used to denote the software overheads of a communication protocol. Though we are aware that δ depends on the data transfer size, the time difference is negligible, compared to the time of actual data transfer and processing. Therefore, for the sake of simplicity, δ is a constant in our model.

Note that in our definition of a single pipe there is only one terminal, not two at either end of the pipe. This differs from the idea of a POSIX pipe, which comprises a task at both sending and receiving ends. In our case, a pipe is represented by the single terminal that takes input and produces output.

An example of two communicating pipes is shown in Figure 3. This is representative of a communication path between a gyro task and attitude calculation in Cleanflight on the Aero board. The gyro task is mapped to Pipe 1, whose input end is over the SPI bus connected to the gyro sensor and output end is over a region of memory shared with Pipe 2. Pipe 1's terminal is an I/O VCPU because the gyro task is responsible for handling I/O interrupts generated from the SPI bus. On the contrary, the terminal of Pipe 2 is a Main VCPU as the AHRS task is CPU-intensive. The gyro task reads raw gyro readings from Pipe 1's input end, processes them, and writes filtered gyro readings to Pipe 1's output end. Similarly, the AHRS task reads the filtered gyro readings from Pipe 2's input end and produces attitude data for its output end over shared memory.

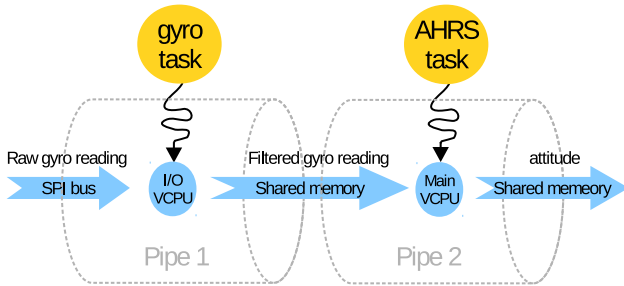


Fig. 3. Illustration of Two Communicating Pipes

1) *Notation*: The timing characteristics of a pipe are denoted by the 3-tuple, $\pi = ((W_i, \delta_i), (C, T), (W_o, \delta_o))$, where:

- (W_i, δ_i) and (W_o, δ_o) denote the bandwidth and software overheads of the input and output ends, respectively.
- (C, T) denotes the budget and period of the pipe terminal.

A task τ is also denoted as a 3-tuple, $\tau = (d_i, p, d_o)$, where:

- d_i denotes the size of the raw data that is read in by τ in order to perform its job, and d_o denotes the size of the processed data that is produced by τ .
- p denotes the uninterrupted processing time it takes for τ to turn the raw data into the processed data.

In addition, $\tau \mapsto \pi$ denotes the mapping between task τ and pipe π . A task $\tau = (d_i, p, d_o)$ is said to be mapped to a pipe $\pi = ((W_i, \delta_i), (C, T), (W_o, \delta_o))$ when

- data of size d_i is read from the input end with parameters (W_i, δ_i) , and data of size d_o is written to the output end with parameters (W_o, δ_o) ;

- the pipe terminal with parameters (C, T) is used for scheduling and accounting of the read and write operations, as well as the processing that takes time p .

For the composition of a chain of pipes, the operator $|$ connects a pipe's output end to its succeeding pipe's input end. For example, Figure 3 is represented as $\tau_{gyro} \mapsto \pi_1 | \tau_{AHRS} \mapsto \pi_2$. The scheduling latency between two pipes is denoted by $S_{\tau_1 \mapsto \pi_1 | \tau_2 \mapsto \pi_2}$. Lastly, given a task set $T = \{\tau_1, \tau_2, \dots, \tau_n\}$ identity mapped to a pipe set $\Pi = \{\pi_1, \pi_2, \dots, \pi_n\}$, where pipes are connected to each other in ascending order of subscript, $E_{\tau_1 \mapsto \pi_1 | \tau_2 \mapsto \pi_2 | \dots | \tau_n \mapsto \pi_n}$ denotes the end-to-end reaction time of the pipe chain, and $F_{\tau_1 \mapsto \pi_1 | \tau_2 \mapsto \pi_2 | \dots | \tau_n \mapsto \pi_n}$ denotes the end-to-end freshness time.

D. Reachability

Before mathematically analyzing end-to-end time, we introduce the concept of *reachability*, inspired by the *data-path reachability conditions* proposed by Feiertag et al [11]. The need to consider reachability is due to a subtle difference between our register-based asynchronous communication model and the traditional FIFO-based synchronous communication. In the latter, data is guaranteed to be transferred without loss or repetition. This way, end-to-end time is derived from the time interval between the arrival of a data input and the departure of its *corresponding* data output. Unfortunately, this might result in an infinitely large end-to-end time in the case of register-based asynchronous communication where not every input leads to an output. Instead, unprocessed input data might be discarded (overwritten) when newer input data is available, as explained in Section II-C.

An infinitely large end-to-end time, while mathematically correct, lacks practical use. Therefore, the following timing analysis ignores all input data that fails to “reach” the exit of the pipe chain it enters. Instead, only those data inputs that result in data outputs from the pipe chain are considered. We define this latter class of inputs as being *reachable*.

E. Timing Analysis

As alluded to above, the execution of a task is divided into three stages, involving (1) reading, (2) processing, and (3) writing data. To simplify the timing analysis, we assume that tasks are able to finish the read and write stages within one period of the pipe terminal, to which the task is mapped. This is not unrealistic for applications such as a flight controller, because: 1) data to be transferred is usually small, and 2) all three stages are typically able to finish within one period. However, to maintain generality, we do not impose any restriction on the length of the processing stage.

1) *Worst-case End-to-end Time of a Single Pipe*: First, we consider the case where there is a single pipe. Two key observations for this case are: 1) the absence of scheduling latency due to the lack of a succeeding pipe, and 2) the equivalence of the two end-to-end time semantics (reaction and freshness time) due to the lack of a preceding pipe. We therefore use $L_{\tau \mapsto \pi}$ to unify the notation of $E_{\tau \mapsto \pi}$ and $F_{\tau \mapsto \pi}$.

Given task $\tau = (d_i, p, d_o)$ mapped to pipe $\pi = ((W_i, \delta_i), (C, T), (W_o, \delta_o))$, the worst-case end-to-end time is

essentially the execution time of the three stages of τ on π . Due to the timing property of π 's pipe terminal, τ is guaranteed C units of execution time within any window of T time units. Hence, the worst-case latency $L_{\tau \mapsto \pi}^{wc}$ is bounded by the following:

$$L_{\tau \mapsto \pi}^{wc} = \left\lceil \frac{\Delta_{in} + p + \Delta_{out}}{C} \right\rceil \cdot T + (\Delta_{in} + p + \Delta_{out}) \bmod C \quad (1)$$

where $\Delta_{in} = \frac{d_i}{W_i^p} + \delta_i$ and $\Delta_{out} = \frac{d_o}{W_o^p} + \delta_o$.

2) *Worst-case End-to-end Reaction Time of a Pipe Chain:* In this section, we extend the timing analysis of a single pipe to a pipe chain. For the sake of simplicity, we start with a chain of length two. We show in Section III-F that the mathematical framework is applicable to arbitrarily long pipe chains. To distinguish the tasks mapped to the two pipes, we name the preceding task producer and the succeeding consumer. The producer is denoted by $\tau_p = (d_i^p, p^p, d)$ and its pipe is denoted by $\pi_p = ((W_i^p, \delta_i^p), (C^p, T^p), (W_o^p, \delta_o^p))$. Similarly, the consumer task and pipe are denoted by $\tau_c = (d, p^c, d_o^c)$ and $\pi_c = ((W_i^c, \delta_i^c), (C^c, T^c), (W_o^c, \delta_o^c))$. Following the definition of the end-to-end reaction time, $E_{\tau_p \mapsto \pi_p | \tau_c \mapsto \pi_c}$, in Section III-A, we investigate the time interval between a specific instance of input data, denoted by D_i , being read by τ_p , and its **first** corresponding output, denoted by D_o , being written by τ_c .

It is of vital importance to recognize that end-to-end time of a pipe chain is not simply the sum of the end-to-end time of each single pipe in the chain. We also need to account for the scheduling latency resulting from each appended pipe. As described in Section III-B, the scheduling latency depends on the order of execution of tasks. We, therefore, perform the timing analysis under two complementary cases: **Case 1** - τ_c has shorter period and thus higher priority than τ_p ; **Case 2** - τ_p has shorter period and thus higher priority than τ_c , according to rate-monotonic ordering.

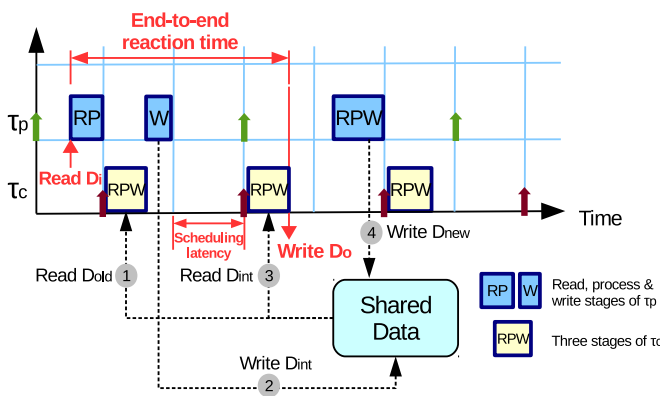


Fig. 4. End-to-end Reaction Time in Case 1

a) Calculating the End-to-end Reaction Time: Case 1.

The key to making use of $L_{\tau_p \mapsto \pi_p}^{wc}$ and $L_{\tau_c \mapsto \pi_c}^{wc}$ in the timing analysis of $E_{\tau_p \mapsto \pi_p | \tau_c \mapsto \pi_c}^{wc}$, is to find the worst-case scheduling latency, $S_{\tau_p \mapsto \pi_p | \tau_c \mapsto \pi_c}^{wc}$. As illustrated in Figure 4, the worst-case scheduling latency occurs when τ_c preempts τ_p (Step

①) immediately before τ_p produces the intermediate output D_{int} corresponding to D_i . After preemption, τ_c uses up π_c 's budget and gives the CPU back to τ_p . Upon being resumed, τ_p immediately produces D_{int} (Step ②). For τ_c to become runnable again to read D_{int} in Step ③, it has to wait for its budget replenishment. The waiting time is exactly the worst-case scheduling latency:

$$S_{\tau_p \mapsto \pi_p | \tau_c \mapsto \pi_c}^{wc} = T^c - C^c - \left(\frac{d}{W_o^p} + \delta_o^p \right) \quad (2)$$

After replenishment, τ_c reads in D_{int} , processes it and eventually writes out D_o . As $E_{\tau_p \mapsto \pi_p | \tau_c \mapsto \pi_c}$ is defined to be the time interval between the arrival of D_i and the departure of D_o , the worst case of $E_{\tau_p \mapsto \pi_p | \tau_c \mapsto \pi_c}$ is as follows:

$$\begin{aligned} E_{\tau_p \mapsto \pi_p | \tau_c \mapsto \pi_c}^{wc} &= L_{\tau_p \mapsto \pi_p}^{wc} + S_{\tau_p \mapsto \pi_p | \tau_c \mapsto \pi_c}^{wc} + L_{\tau_c \mapsto \pi_c}^{wc} \\ &= L_{\tau_p \mapsto \pi_p}^{wc} + L_{\tau_c \mapsto \pi_c}^{wc} + T^c - C^c - \left(\frac{d}{W_o^p} + \delta_o^p \right) \end{aligned} \quad (3)$$

Note that if τ_c runs out of budget before writing D_o , τ_p may overwrite D_{int} in the pipe with new data (Step ④). However, the *implicit communication* property guarantees that τ_c only works on its local copy of the shared data, which is D_{int} until τ_c initiates another read.

Case 2. The situation is more complicated when τ_p has higher priority than τ_c . The worst-case scenario in Case 1 does not hold in Case 2 primarily because τ_p might overwrite D_{int} before τ_c has a budget replenishment. This is impossible in Case 1 because τ_p has a larger period than τ_c , which is guaranteed to have its budget replenished before τ_p is able to initiate another write. In other words, in Figure 4, Step ③ is guaranteed to happen before Step ④.

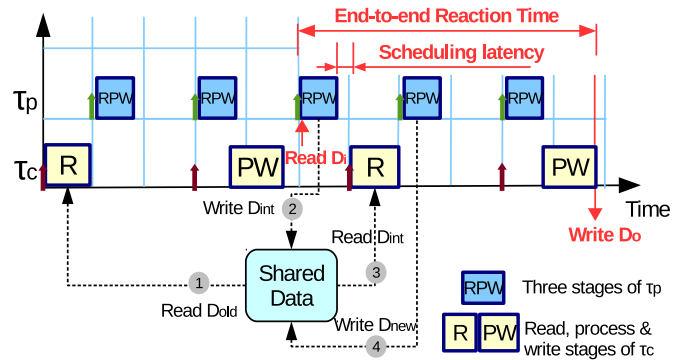


Fig. 5. End-to-end Reaction Time in Case 2

The data-overwrite problem in Case 2 is the reason for introducing reachability in Section III-D. To find the worst-case end-to-end reaction time in this case, we have to find the scenario that not only leads to the worst-case scheduling latency, but also originates from a *reachable* input. Figure 5 illustrates a scenario that meets these requirements. In the figure, τ_p preempts τ_c immediately after τ_c finishes reading τ_p 's intermediate output (Step ③), D_{int} , corresponding to D_i . It follows that the longest possible waiting time, between D_{int} becoming available (Step ②) and τ_c reading the data

(Step ③), is the period of τ_p minus both its budget and the execution time of the read stage of τ_c . This waiting time is exactly the worst-case scheduling latency:

$$S_{\tau_p \mapsto \pi_p | \tau_c \mapsto \pi_c}^{wc} = T^p - C^p - \left(\frac{d}{W_i^c} + \delta_i^c \right) \quad (4)$$

Between reading D_{int} and writing D_o , τ_c might experience more than one preemption from τ_p , which repeatedly overwrites the shared data. This will not, however, affect τ_c 's processing on D_{int} either spatially or temporally, thanks to the VCPU model and the implicit communication semantic. Similar to Case 1, the worst-case end-to-end reaction time is again the sum of Equation 1 of each pipe and Equation 4:

$$\begin{aligned} E_{\tau_p \mapsto \pi_p | \tau_c \mapsto \pi_c}^{wc} &= L_{\tau_p \mapsto \pi_p}^{wc} + S_{\tau_p \mapsto \pi_p | \tau_c \mapsto \pi_c}^{wc} + L_{\tau_c \mapsto \pi_c}^{wc} \\ &= L_{\tau_p \mapsto \pi_p}^{wc} + L_{\tau_c \mapsto \pi_c}^{wc} + T^p - C^p - \left(\frac{d}{W_i^c} + \delta_i^c \right) \end{aligned} \quad (5)$$

Since the output end of τ_p and the input end of τ_c share the same communication channel, it is reasonable to assume that $W_o^p = W_i^c$ and $\delta_o^p = \delta_i^c$. With that, we proceed to unify the worst-case end-to-end reaction time as follows:

$$E_{\tau_p \mapsto \pi_p | \tau_c \mapsto \pi_c}^{wc} = \begin{cases} T^c - C^c - \left(\frac{d}{W} + \delta \right) \\ + L_{\tau_p \mapsto \pi_p}^{wc} + L_{\tau_c \mapsto \pi_c}^{wc}, & \text{if } T^c < T^p \\ T^p - C^p - \left(\frac{d}{W} + \delta \right) \\ + L_{\tau_p \mapsto \pi_p}^{wc} + L_{\tau_c \mapsto \pi_c}^{wc}, & \text{otherwise} \end{cases} \quad (6)$$

where $W = W_o^p = W_i^c$ and $\delta = \delta_o^p = \delta_i^c$

b) *Special Cases:* Real-time systems are often profiled offline to obtain worst-case execution times of their tasks. In our case, this would enable CPU resources for pipe terminals to be provisioned so that each task completes one iteration of all three stages (read, process, write) in one budget allocation and, hence, period. This implies that $\Delta_{in} + p + \Delta_{out} + \epsilon = C$ in Equation 1, where ϵ is an arbitrarily small positive number to account for surplus budget after completing all task stages. With that, it is possible to simplify the worst-case end-to-end reaction time derived in Section III-E2a. First, Equation 1 is simplified as follows:

$$\begin{aligned} L_{\tau \mapsto \pi}^{wc} &= \left\lfloor \frac{C - \epsilon}{C} \right\rfloor \cdot T + [(C - \epsilon) \bmod C] \\ &= 0 \cdot T + (C - \epsilon) \approx C \end{aligned} \quad (7)$$

Using Equation 7, Equation 5 reduces to:

$$\begin{aligned} E_{\tau_p \mapsto \pi_p | \tau_c \mapsto \pi_c}^{wc} &= T^p - C^p - \Delta_{in}^c + L_{\tau_p \mapsto \pi_p}^{wc} + L_{\tau_c \mapsto \pi_c}^{wc} \\ &= T^p - C^p - \Delta_{in}^c + C^p + C^c \\ &= T^p + C^c - \Delta_{in}^c \end{aligned} \quad (8)$$

The same simplification applied to Equation 3 of Case 1 reduces Equation 6 to:

$$E_{\tau_p \mapsto \pi_p | \tau_c \mapsto \pi_c}^{wc} = \begin{cases} T^c + C^p - \Delta, & \text{if } T^c < T^p \\ T^p + C^c - \Delta, & \text{otherwise} \end{cases} \quad (9)$$

where $\Delta = \frac{d}{W} + \delta$.

If we further assume that π_p and π_c communicate data of small size over shared memory, it is possible to discard

communication overheads, such that $\Delta = 0$. With that, Equation 9 simplifies to:

$$E_{\tau_p \mapsto \pi_p | \tau_c \mapsto \pi_c}^{wc} = \begin{cases} T^c + C^p, & \text{if } T^c < T^p \\ T^p + C^c, & \text{otherwise} \end{cases} \quad (10)$$

Finally, notice that by appending $\tau_c \mapsto \pi_c$ to $\tau_p \mapsto \pi_p$, the worst-case end-to-end reaction time is increased by the following:

$$\begin{aligned} \uparrow E^{wc} &= E_{\tau_p \mapsto \pi_p | \tau_c \mapsto \pi_c}^{wc} - E_{\tau_p \mapsto \pi_p}^{wc} \\ &= E_{\tau_p \mapsto \pi_p | \tau_c \mapsto \pi_c}^{wc} - C^p \\ &= \begin{cases} T^c, & \text{if } T^c < T^p \\ T^p - C^p + C^c, & \text{otherwise} \end{cases} \end{aligned} \quad (11)$$

3) *Worst-case End-to-end Freshness Time of a Pipe Chain:* Techniques similar to those in Section III-E2 will be used to analyze end-to-end freshness time. To avoid repetition, we abbreviate the end-to-end freshness timing analysis by only focusing on the special cases described in Section III-E2b.

Recall that freshness time is defined to be the interval between the arrival of an input and the departure of its *last corresponding* output. Therefore, we investigate the interval between a specific instance of input data, D_i , being read by τ_p and its *last* corresponding output, D_o , being written by τ_c .

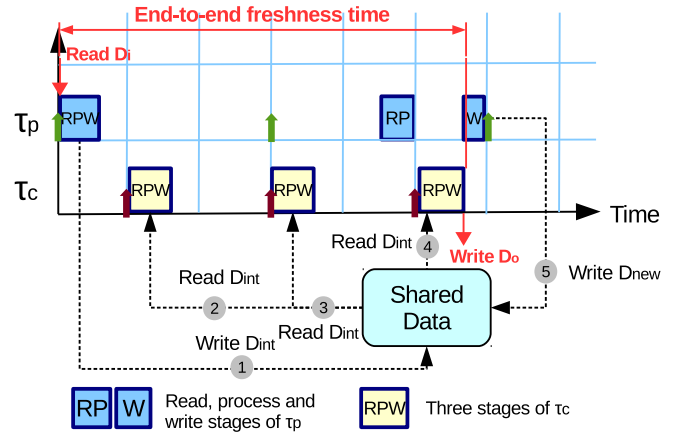


Fig. 6. End-to-end Freshness Time in Case 1

Case 1. As illustrated in Figure 6, D_i is read by the first instance of τ_p at time 0 and the intermediate output, D_{int} , is written to the shared data (Step ①). After that, τ_c produces three outputs corresponding to D_{int} (Steps ②, ③ and ④), or to D_i indirectly. The last output, D_o , is the one preceding τ_p 's write of new data, D_{new} (Step ⑤). Thus, the worst-case end-to-end freshness time, $F_{\tau_p \mapsto \pi_p | \tau_c \mapsto \pi_c}^{wc}$, occurs when: 1) the two consecutive writes (Steps ① and ⑤) from τ_p have the longest possible time interval between them, and 2) the write of D_o happens as late as possible. The latest time to write D_o is immediately before the second write of τ_p , which is preempted by higher priority τ_c .

From Figure 6 that the worst-case end-to-end freshness time is:

$$F_{\tau_p \mapsto \pi_p | \tau_c \mapsto \pi_c}^{wc} = 2 \cdot T^p - \Delta_{out}^p \quad (12)$$

Again, when communicating over shared memory, Equation 12 can be further simplified to:

$$F_{\tau_p \mapsto \pi_p | \tau_c \mapsto \pi_c}^{wc} = 2 \cdot T^p \quad (13)$$

Case 2. When τ_p has a smaller period than τ_c , it is impossible for τ_c to read the same intermediate output of τ_p twice. In Figure 6, Step ⑤ is guaranteed to happen before ③. Thus, the worst-case freshness time is essentially the worst-case reaction time, shown in Equation 5.

In summary, the worst-case end-to-end freshness latency of two communicating pipes is represented in the following conditional equation:

$$F_{\tau_p \mapsto \pi_p | \tau_c \mapsto \pi_c} = \begin{cases} 2 \cdot T^p, & \text{if } T^c < T^p \\ T^p + C^c, & \text{otherwise} \end{cases} \quad (14)$$

F. Composability

The timing analysis for two pipes in Section III-E2 extends to pipe chains of arbitrary length. Every time an extra task τ_{new} (mapped to π_{new}) is appended to the tail end of a chain ($\tau_{tail} \mapsto \pi_{tail}$), the worst-case end-to-end reaction time increases by the worst-case end-to-end time of the newly appended pipe, plus the scheduling latency between the new pipe and the tail pipe. The actual value of the increase, depending on the relative priority of the new pipe and the tail pipe, is shown in Equation 11. Similarly, the added end-to-end freshness time can be derived from Equation 14.

Composability is a crucial property of our pipe model, since it significantly eases the end-to-end time calculation for any given pipeline. This provides the basis for a design framework that derives task periods from given end-to-end timing constraints. This is detailed in the following section.

IV. END-TO-END DESIGN

There are significant challenges to porting a flight control firmware such as Cleanflight to run as a multithreaded application on a real-time operating system. One of the major issues is how to determine the period of each thread so that the application is able to meet its end-to-end timing constraints. A naive approach would be to start by choosing a tentative set of periods and use the timing analysis method in Section III to validate the timing correctness. Upon failure, the periods are heuristically adjusted and the validation step is repeated until end-to-end timing guarantees are met. This approach, however, is potentially time-consuming and labor-intensive when the number of tasks or constraints increase.

Inspired by Gerber *et al* [12], we derive task periods from end-to-end timing constraints, by combining the timing analysis of the pipe model with linear optimization techniques. In this section, we generalize our method for use with a broader spectrum of cyber-physical control applications.

A. Problem Definition

Consider a set of tasks $\Gamma = \{\tau_1, \tau_2, \dots, \tau_n\}$ and a set of pipes $\Pi = \{\pi_1, \pi_2, \dots, \pi_n\}$, where $\tau_j = (d_i^j, p^j, d_o^j)$ and

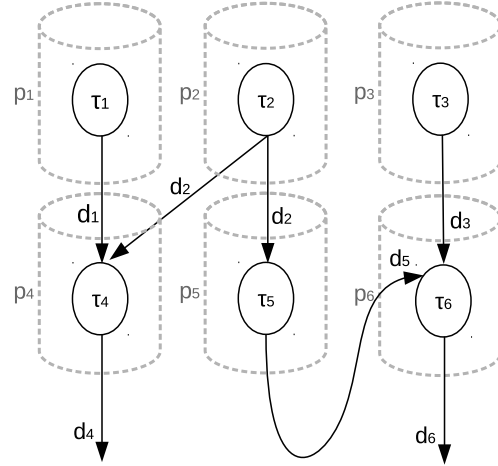


Fig. 7. Application Task Graph

Reaction	Freshness
$E_{\tau_1 \mapsto \pi_1 \tau_4 \mapsto \pi_4} \leq 10,$ $E_{\tau_2 \mapsto \pi_2 \tau_4 \mapsto \pi_4} \leq 15,$ $E_{\tau_2 \mapsto \pi_2 \tau_5 \mapsto \pi_5 \tau_6 \mapsto \pi_6} \leq 25,$ $E_{\tau_3 \mapsto \pi_3 \tau_6 \mapsto \pi_6} \leq 15;$	$F_{\tau_1 \mapsto \pi_1 \tau_4 \mapsto \pi_4} \leq 20,$ $F_{\tau_2 \mapsto \pi_2 \tau_4 \mapsto \pi_4} \leq 30,$ $F_{\tau_2 \mapsto \pi_2 \tau_5 \mapsto \pi_5 \tau_6 \mapsto \pi_6} \leq 50,$ $F_{\tau_3 \mapsto \pi_3 \tau_6 \mapsto \pi_6} \leq 20;$
Schedulability	Execution Time
$\sum_{j=1}^6 \frac{C^j}{T^j} \leq 6(\sqrt[6]{2} - 1)$	$\forall j \in \{1, 2, \dots, 6\},$ $d_i^j = d_o^j = 3,$ $W_i^j = W_o^j = 20,$ $\delta_i^j = \delta_o^j = 0.1,$ $p^j = 0.5;$

TABLE II
APPLICATION TIMING CHARACTERISTICS

$\pi_j = ((W_i^j, \delta_i^j), (C^j, T^j), (W_o^j, \delta_o^j))$. We additionally require the following information:

- the mapping between Γ and Π . For ease of notation, we assume tasks map to the pipe with the same subscript, hence $\forall j \in \{1, 2, \dots, n\}, \tau_j \mapsto \pi_j$;
- the topology of Π (an example is shown in Figure 7);
- $\forall j \in \{1, 2, \dots, n\}$, the value of d_i^j , p^j and d_o^j ;
- $\forall j \in \{1, 2, \dots, n\}$, the value of W_i^j , δ_i^j , W_o^j and δ_o^j ;
- the end-to-end timing constraints, namely the value of $E_{\tau_i \mapsto \pi_i | \tau_j \mapsto \pi_j | \dots | \tau_k \mapsto \pi_k}$ and/or $F_{\tau_p \mapsto \pi_p | \tau_q \mapsto \pi_q | \dots | \tau_r \mapsto \pi_r}$ where $i, j, k, p, q, r \in \{1, 2, \dots, n\}$.

The aim is to find a feasible set of $\{(C^j, T^j)\}$ pairs for $j \in \{1, 2, \dots, n\}$ that: (1) meets all the specified end-to-end timing constraints, (2) passes the task schedulability test, and (3) ideally but not necessarily minimizes CPU utilization. A task should not be run faster than necessary, to free resources for additional system objectives.

B. Solving the Constraints

Our solution is carried out in a three-step process. To make it easier to understand, we use a concrete example with actual numbers to elaborate the process. Consider the pipe topology graph shown in Figure 7, in which there are six tasks mapped to six pipes. Tasks 1, 2 and 3 read inputs from sensors, Tasks 4 and 6 write their outputs to actuators, and Task 5 is an intermediary responsible for complicated processing such as

PID control or sensor data fusion. The timing characteristics of the tasks and pipes are shown in Table II. Note that the execution times are assumed to be identical for all tasks. In practice this would not necessarily be the case but it does not affect the generality of the approach.

In Step 1, we use the given d_i , d_o , p , W_i , δ_i , W_o and δ_o to compute the budget of each pipe terminal. The budget is set to a value that ensures the three stages (*i.e.*, read, process and write) finish in one period. To compute C^1 , for example, we aggregate the times for τ_1 to read, process and write data. Thus $C^1 = \frac{d_1^1}{W_i^1} + \delta_i^1 + p^1 + \frac{d_o^1}{W_o^1} + \delta_o^1$. All budgets are computed in a similar way.

When the input to a pipe terminal comes from multiple sources the value d_i is aggregated from all input channels. For example, τ_4 receives a maximum of $d_4^i = d_1 + d_2$ amount of data every transfer from both τ_1 and τ_2 . Data from a pipe terminal is not necessarily duplicated for all pipe terminals that are consumers. For example, τ_2 generates a maximum of $d_o^2 = d_2$ data every transfer, by placing a single copy of the output in a shared memory region accessible to both τ_4 and τ_5 . If the communication channels did not involve shared memory, then data would be duplicated, so that $d_o^2 = 2d_2$.

In Step 2, we derive a list of inequations involving period variables from the given end-to-end timing and scheduling constraints in Table II. For simplicity, the scheduling constraint is shown as a rate-monotonic utilization bound on the six pipe tasks. However, for sensor inputs and some actuator outputs, Quest would map those tasks to I/O VCPUs that have a different utilization bound, as described in our earlier work [7].

The derivation is based on Equations 9 and 14, and the composability property of the pipe model. According to the conditional equations, however, every two pipes with undetermined priority can lead to two possible inequations. This exponentially increases the search space for feasible periods. In order to prune the search space, our strategy is to always start with the case where $T^p > T^c$. This is based on the observation that tasks tend to over-sample inputs for the sake of better overall responsiveness. Thus, the reaction constraint $E_{\tau_2 \mapsto \pi_2 | \tau_5 \mapsto \pi_5 | \tau_6 \mapsto \pi_6} \leq 25$, for example, is translated to inequation $T^5 + C^2 - \Delta + T^6 \leq 25$. This is derived by combining Equations 9 and 11. It is then possible to translate all timing constraints to inequations with only periods as variables. In addition, periods are implicitly constrained by $T^j > C^j, \forall j \in \{1, 2, \dots, n\}$.

Given all the inequations, Step 3 attempts to find the maximum value for each period so that the total CPU utilization is minimized. We are then left with a linear programming problem. Unfortunately, there is no polynomial time solution to the integer linear programming problem, as it is known to be NP-hard. Though solutions are possible under certain mathematical conditions [13], this is beyond the scope of this paper. Instead, in practice, the problem can be simplified because 1) there are usually a small number of fan-in and fan-out pipe ends for each task, meaning that a period variable is usually involved in a small number of inequations, and 2) a sensor task period is usually pre-determined by a hardware sampling rate limit. For example, if we assume T^3 is known

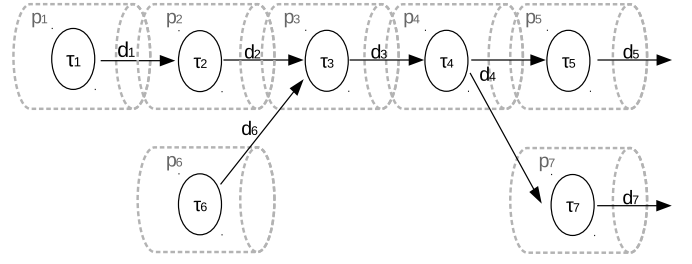


Fig. 8. Simulation Pipe Topology

to be 5, a feasible set of periods for the example in Table II is easily found: $\{T^1 = 10, T^2 = 15, T^3 = 10, T^4 = 10, T^5 = 15, T^6 = 5\}$. If we ignore the integer requirement, it is possible to find a feasible solution in polynomial time using rational numbers rounded to integers. Though rounding may lead to constraint violations, it is possible to increase the time resolution to ensure system overheads exceed those of rounding errors. If all else fails, one can resort to an exhaustive search of all possible constraint solutions.

Note that the above approach aims to find a feasible, rather than optimal, set of task periods. An optimal solution depends on which constraints (freshness, reaction time, or schedulability) are more important, which is out of the scope of this paper.

V. EVALUATION

This section describes experiments on the Intel Aero board with an Atom x7-Z8750 1.6 GHz 4-core processor and 4GB RAM.

A. Simulation Experiments

We developed simulations for both Linux and Quest, to predict the worst-case end-to-end time using the equations in Section III. The simulations consist of seven tasks, all of which search for prime numbers within a certain range and then communicate with one another to exchange their results. Each of the tasks is mapped to a separate pipe. The topology of the pipes is shown in Figure 8. The communication channel is shared memory with caches disabled and the data size is set to 6.7 KB to achieve a non-negligible 1 millisecond communication overhead. Each task is assigned a different search range and the profiled execution time is shown in Table III in milliseconds. The budget of each pipe is set to be slightly larger than the execution time of its corresponding task, to compensate for system overheads. The settings of each pipe terminal (PT) are also shown in Table III, again in milliseconds. Apart from the seven main tasks, the system is loaded with low priority background tasks that consume all the remaining CPU resources.

τ_1	τ_2	τ_3	τ_4	τ_5	τ_6	τ_7
11.5	5.5	3.5	5.5	11.5	11.5	3.5
PT 1	PT 2	PT 3	PT 4	PT 5	PT 6	PT 7
(12,100)	(6,50)	(4,150)	(6,100)	(12,150)	(12,100)	(4,50)

TABLE III
SIMULATION SETTINGS

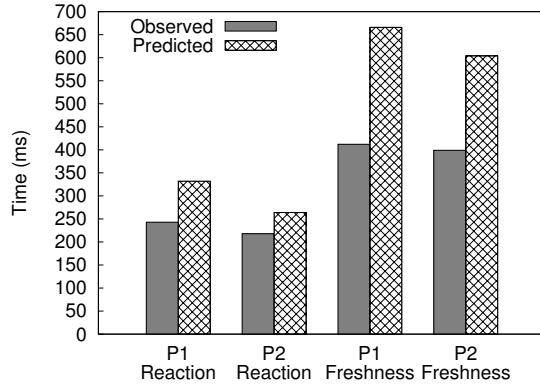


Fig. 9. Observed vs. Predicted Freshness & Reaction Times

We measure the end-to-end reaction time and freshness time separately, for pipeline $p_1 \rightarrow p_2 \rightarrow p_3 \rightarrow p_4 \rightarrow p_5$ (denoted by P1), and $p_6 \rightarrow p_3 \rightarrow p_4 \rightarrow p_7$ (denoted by P2), and compare them to corresponding theoretical bounds. Figure 9 shows the results after 100,000 outputs are produced by τ_5 and τ_7 , respectively on Quest. As can be seen, the observed values are always within the prediction bounds.

The difference between observed and predicted freshness times is greater than between observed and predicted reaction times. This is because our strategy for deriving feasible task periods starts with producers having greater periods than consumers. As stated in Section III-A, the freshness time is affected by the period of each producer, so the prediction may not be as tight as for reaction time.

We also perform the same experiment on Yocto Linux shipped with the Aero board. The kernel is version 4.4.76 and patched with the PREEMPT_RT patch. While running the simulation, the system also uncompresses Linux source code in the background. This places the same load on the system as the background tasks in Quest. Figure 10 summarizes the average reaction time (AVGR), worst-case reaction time (WCR), maximum variance of reaction time (MaxRV), average freshness time (AVGF), worst-case freshness time (WCF) and maximum variance of freshness time (MaxFV) of pipeline P1 for Quest and Linux. Compared to Linux, there is less variance shown by the end-to-end times using Quest. Additionally, the freshness and reaction times are lower than with Linux.

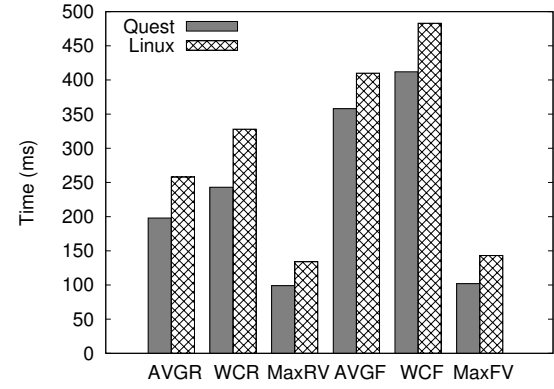


Fig. 10. Quest vs. Linux End-to-end Times

UART serial, and pulse-width modulation (PWM). Quest currently uses the I/O hub to send PWM signals to electronic speed controllers (ESCs) that alter motor and, hence, drone rotor speeds. We modified the FPGA logic to improve the timing resolution of PWM signals, as well as control their duty cycle and periods. We also wrote drivers to use an on-board Bosch BMI160 Inertial Measurement Unit (IMU). Both the I/O hub and IMU connect to the main processor via an SPI bus.

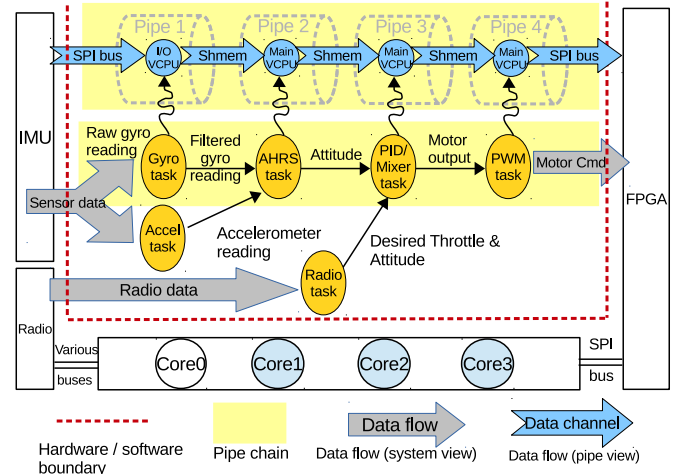


Fig. 11. Cleanflight Data Flow

B. The Cleanflight Experiment

Our next experiments apply the end-to-end design approach to determining the periods of each task in the re-implementation of Cleanflight. The flight controller is refactored as a multithreaded application running on the Intel Aero board. The hardware and software architecture is shown in Figure 11.

Hardware. We currently only use Core 0 to run Cleanflight on Quest. The remaining three cores are reserved for future development of a complete autonomous flight management system. Apart from the CPU, the Aero board also has an FPGA-based I/O coprocessor. It provides FPGA-emulated I/O interfaces including analog-to-digital conversion (ADC),

Software. To avoid writing further device drivers, we disabled non-time-critical auxiliary features of Cleanflight such as telemetry, blackbox data logging, and UART-based flight control configuration. The essential components are shown as circular tasks in Figure 11. The AHRS sensor fusion task takes the input readings of the accelerometer and gyroscope (in the BMI160 IMU) and calculates the current attitude of the drone. Then, the PID task compares the calculated and target attitudes, and feeds the difference to the PID control logic. In the original Cleanflight code, the target attitude is determined by radio-control signals from a human flying the drone. In an autonomous setting, the target attitude would be calculated according to on-board computations based on mission objectives and flight conditions. The output is nonetheless mixed with the

desired throttle and read in by the PWM task, which translates it to motor commands. Motor commands are sent over the SPI bus and delivered as PWM signals to each ESC associated with a separate motor-rotor pair on the drone. We decouple all these tasks into separate threads. For safety reasons, the sensor and PWM tasks are given individual address spaces. For simplicity, we use a synthetic radio input value (20% throttle and 0 degree pitch, roll, and yaw angle) instead of reading from the real radio driver. The tasks are profiled and execution times are shown in Table IV.

	Gyro	AHRS	PID	PWM	Accl	Radio
Exec Times (μ s)	174	10	2	970	167	12

TABLE IV
TASK EXECUTION TIMES

As can be seen in Figure 11, there are three data paths, originating from the gyro, accelerometer, and radio receiver, respectively. Unfortunately, there is little information available on what end-to-end timing constraints should be imposed on each path to guarantee a working drone. Most timing parameters in the original Cleanflight are determined by trial and error. Instead of determining the optimum timing constraints, the focus of this paper is on guaranteeing given constraints. Therefore, we first port Cleanflight to Yocto Linux on the Aero board, as a reference implementation. The Linux version remains single-threaded and is used to estimate the desired end-to-end time. For example, for the gyro path, the worst-case reaction and freshness times are measured to be 9769 and 22972 μ s, respectively. We round them to 10 and 23 ms, and use them as end-to-end timing constraints for our flight controller implementation. Using the same approach, we determine end-to-end reaction and freshness times for the accelerometer path, which are set to 10 and 23 ms, respectively. Finally, for the radio path, we set the end-to-end reaction and freshness times to be 20 and 44 ms, respectively.

Using the execution times in Table IV and timing constraints above, we apply the end-to-end design approach to derive the periods. The results for each task are shown in Table V. Note that there are four extra tasks inherited from the original Cleanflight. They are responsible for checking system utilization, battery current and voltage, and emitting low battery alerts. However, they are not on the critical control path and we run them only when there is surplus CPU time. Thus for brevity, they are not shown in Figure 11 and not involved in the period calculation.

Task	Gyro	AHRS	PID
Budget/Period (μ s)	200/1000	100/5000	100/2000
Task	PWM	Accl	Radio
Budget/Period (μ s)	1000/5000	200/1000	100/10000

TABLE V
TASK PERIODS

Evaluation. To measure the actual end-to-end time, we focus on the longest pipe chain highlighted in Figure 11. We instrument the Cleanflight code to append every gyro reading with an incrementing ID, and also record a timestamp before the gyro input is read. The timestamp is then stored in an array indexed by the ID. Every task is further instrumented to maintain the ID when translating input data to output. This

way, the ID is preserved along the pipe chain, from the input gyro reading to the output motor command. After the PWM task sends out motor commands, it looks up the timestamp using its ID and compares it to the current time. By doing this, we are able to log both the reaction and freshness end-to-end time for every input gyro reading. We then compare the observed end-to-end time with the given timing constraints, as well as the predicted worst-case value. Results are shown in Figure 12. As can be seen, the observed values are always within the predicted bounds, and always meet the timing constraints.

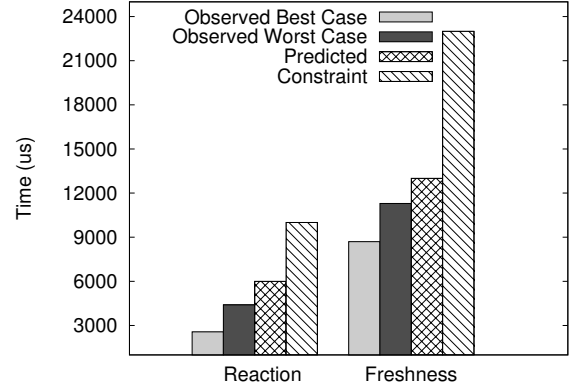


Fig. 12. Cleanflight Times

VI. RELATED WORK

Feiertag *et al.* [11] distinguish four semantics of end-to-end time and provide a generic framework to determine all the valid data paths for each semantic. The authors do not perform timing analysis as no scheduling model is assumed. Hamann *et al.* [10] also discuss end-to-end reaction and age time. Their work focuses on integrating three different communication models, including the implicit communication model, into existing timing analysis tools such as SymTA/S [14]. While our composable pipe model is also based on implicit communication, we perform timing analysis for a sequence of RMS-scheduled tasks running on bandwidth-preserving servers.

Others have proposed end-to-end timing analysis at the model level in the automotive domain [15], [16]. Our approach is applicable to any applications with data pipeline processing, freshness and reaction constraints. A large portion of end-to-end reaction time analysis is based on the synchronous data-flow graph (SDFG) [17], where inter-task communication is driven by the arrival of input data. Real-time scheduling techniques have been used to analyze end-to-end latencies in systems modeled by SDFGs [18], [19].

Gerber *et al.* [12] propose a synthesis approach that determines tasks' periods, offsets and deadlines from end-to-end timing constraints. Their work relies on task precedence constraints as there is no scheduling model used for the analysis. Our work uses the Quest scheduling model to perform end-to-end timing analysis. We then derive task periods and budgets to ensure specific reaction, freshness and schedulability constraints.

In contrast to our work, there are programming languages that allow the specification and verification of end-to-end

timing properties. For example, Prelude [20] and Giotto [21] are languages designed to derive tasks' periods based on user-specified timing constraints. Lauer *et al.* [22], [23] use formal methods to verify end-to-end timing properties for avionic systems. Forget *et al.* [24] define a language to specify formally end-to-end constraints and propose a technique to verify those constraints.

VII. CONCLUSIONS & FUTURE WORK

This paper introduces a composable pipe model that is built on task, scheduling and communication abstractions. The pipe model is used to derive a set of task periods and budgets that satisfy both schedulability and end-to-end freshness and reaction timing constraints. We analyze reaction and freshness time in the context of data flow through a task pipeline in a drone flight controller, which performs sensor data processing and motor actuation. Experiments show that Cleanflight ported to the Quest RTOS is able to achieve end-to-end latencies within the predicted time bounds derived by analysis. The scheduling framework in Quest is rich enough to provide bandwidth-guaranteed service to both tasks and interrupt service routines via VCPUs. However, the analysis presented herein is applicable to any OS capable of providing CPU bandwidth guarantees to all task and I/O operations.

Future work will focus on the application of the pipe model to a fully autonomous flight management system involving additional tasks to those in Cleanflight. We intend to use our in-house partitioning hypervisor, called Quest-V [25] to simultaneously host Quest and Linux on the Aero board. Less time-critical tasks such as telemetry, blackbox data logging, path planning and camera-based object detection will be assigned to Linux, to leverage pre-existing device drivers and libraries. Time-critical flight control tasks will then be able to execute without interference in Quest. This avoids the need for a separate control board dedicated to time-critical tasks, which requires space on the drone, and increases weight and power consumption.

ACKNOWLEDGMENT

This work is supported by a gift from Intel Corporation, and the National Science Foundation (NSF) under Grant # 1527050. Any opinions, findings, and conclusions or recommendations expressed in this material are those of the author(s) and do not necessarily reflect the views of the NSF.

REFERENCES

- [1] "Cleanflight: <http://cleanflight.com/>."
- [2] "Quest RTOS: <http://questos.org/>."
- [3] B. Sprunt, "Scheduling Sporadic and Aperiodic Events in a Hard Real-Time System," Software Engineering Institute, Carnegie Mellon, Tech. Rep., 1989.
- [4] C. W. Mercer, S. Savage, and H. Tokuda, "Processor Capacity Reserves for Multimedia Operating Systems," Pittsburgh, PA, Tech. Rep., 1993.
- [5] J. Lehoczky, L. Sha, and Y. Ding, "The Rate Monotonic Scheduling Algorithm: Exact Characterization and Average Case Behavior," in *Proceedings of the IEEE Real-Time Systems Symposium (RTSS)*, 1989.
- [6] C. L. Liu and J. W. Layland, "Scheduling Algorithms for Multiprogramming in a Hard Real-Time Environment," *Journal of the ACM*, vol. 20, no. 1, pp. 46–61, 1973.
- [7] M. Danish, Y. Li, and R. West, "Virtual-CPU Scheduling in the Quest Operating System," in *Proceedings of the 17th Real-Time and Embedded Technology and Applications Symposium*, 2011.
- [8] E. Missimer, K. Missimer, and R. West, "Mixed-Criticality Scheduling with I/O," in *Proceedings of the 28th Euromicro Conference on Real-Time Systems (ECRTS)*, July 2016, pp. 120–130.
- [9] H. Simpson, "Four-slot Fully Asynchronous Communication Mechanism," *IEEE Computers and Digital Techniques*, vol. 137, pp. 17–30, January 1990.
- [10] A. Hamann, D. Dasari, S. Kramer, M. Pressler, and F. Wurst, "Communication Centric Design in Complex Automotive Embedded Systems," in *Proceedings of the 29th Euromicro Conference on Real-Time Systems*, Dagstuhl, Germany, 2017.
- [11] N. Feiertag, K. Richter, J. Nordlander, and J. Jonsson, "A Compositional Framework for End-to-End Path Delay Calculation of Automotive Systems under Different Path Semantics," in *the IEEE RTSS Workshop on Compositional Theory and Technology for Real-Time Embedded Systems*, November 30, 2008.
- [12] R. Gerber, S. Hong, and M. Saksena, "Guaranteeing Real-Time Requirements With Resource-Based Calibration of Periodic Processes," *IEEE Transactions on Software Engineering*, Jul. 1995.
- [13] S. Bradley, A. Hax, and T. Magnanti, *Applied Mathematical Programming*. Addison-Wesley Publishing Company, 1977.
- [14] Rafik Henia and Arne Hamann and Marek Jersak and Razvan Racu and Kai Richter and Rolf Ernst, "System Level Performance Analysis - the SynTA/S Approach," in *IEEE Proceedings Computers and Digital Techniques*, 2005.
- [15] M. Becker, D. Dasari, S. Mubeen, M. Behnam, and T. Nolte, "Synthesizing Job-Level Dependencies for Automotive Multi-rate Effect Chains," in *the 22nd IEEE Intl. Conference on Embedded and Real-Time Computing Systems and Applications*, Aug 2016.
- [16] S. Mubeen, M. Sjödin, T. Nolte, J. Lundbäck, M. Gålnander, and K. L. Lundbäck, "End-to-End Timing Analysis of Black-Box Models in Legacy Vehicular Distributed Embedded Systems," in *the 21st IEEE International Conference on Embedded and Real-Time Computing Systems and Applications*, Aug 2015, pp. 149–158.
- [17] E. A. Lee and D. G. Messerschmitt, "Synchronous Data Flow," *Proceedings of the IEEE*, vol. 75, no. 9, pp. 1235–1245, Sept 1987.
- [18] A. Singh, P. Ekberg, and S. Baruah, "Applying Real-Time Scheduling Theory to the Synchronous Data Flow Model of Computation," in *Proceedings of the 29th Euromicro Conference on Real-Time Systems*, Dagstuhl, Germany, 2017.
- [19] J. Khatib, A. Munier-Kordon, E. C. Klikpo, and K. Trabelsi-Colibet, "Computing Latency of a Real-time System Modeled by Synchronous Dataflow Graph," in *the 24th International Conference on Real-Time Networks and Systems*, ser. RTNS '16. New York, NY, USA: ACM, 2016, pp. 87–96.
- [20] C. Pagetti, J. Forget, F. Boniol, M. Cordovilla, and D. Lesens, "Multi-task Implementation of Multi-periodic Synchronous Programs," *Discrete Event Dynamic Systems*, Sep 2011.
- [21] T. A. Henzinger, B. Horowitz, and C. M. Kirsch, *Giotto: A Time-Triggered Language for Embedded Programming*. Springer Berlin Heidelberg, 2001.
- [22] M. Lauer, F. Boniol, C. Pagetti, and J. Ermont, "End-to-end Latency and Temporal Consistency Analysis in Networked Real-time Systems," *International Journal on Critical Computing-Based Systems*, vol. 5, no. 3/4, 2014.
- [23] F. Boniol, M. Lauer, C. Pagetti, and J. Ermont, "Freshness and Reactivity Analysis in Globally Asynchronous Locally Time-Triggered Systems," in *NASA Formal Methods*. Springer Berlin Heidelberg, 2013.
- [24] J. Forget, F. Boniol, and C. Pagetti, "Verifying End-to-end Real-time Constraints on Multi-periodic Models," in *the 22nd IEEE International Conference on Emerging Technologies and Factory Automation (ETFA)*, Sept 2017, pp. 1–8.
- [25] R. West, Y. Li, E. Missimer, and M. Danish, "A Virtualized Separation Kernel for Mixed-Criticality Systems," *ACM Transactions on Computer Systems*, vol. 34, no. 3, pp. 8:1–8:41, Jun. 2016.